# On the Implementation of Carrierless Amplitude and Phase Modulation in Visible Light Communication

# On the Implementation of Carrierless Amplitude and Phase Modulation in Visible Light Communication

Kabiru O. Akande*, Paul Anthony Haigh† and Wasiu O. Popoola*
*Institute for Digital Communications, School of Engineering, The University of Edinburgh, Edinburgh
{K.Akande,W.Popoola}@ed.ac.uk
† Communications and Information Systems Group, University College London, London, WC1E 6BT, United Kingdom
p.haigh@ucl.ac.uk

***Abstract*—Carrierless amplitude and phase modulation (CAP) is one of the spectrally efficient schemes that has been proposed to tackle the limited modulation bandwidth challenge in visible light communication (VLC). The VLC technology leverages existing lighting fixtures to provide wireless data communication, which makes it attractive for many applications. However, the commercially available white LEDs that are predominantly employed in VLC offer low modulation bandwidths that limit the achievable data rate. Thus, CAP modulation is employed to improve achievable data rate, primarily due to its implementation simplicity and high spectral efficiency. The CAP scheme also has a special feature in that it can be implemented as a single band or a multiband scheme which provides design flexibility. This paper presents an in-depth study of the implementation of CAP in LED-based VLC systems, highlighting the unique features that make it specially suited for VLC applications. Furthermore, a comprehensive investigation is carried out regarding the design parameters of the CAP modulation transceiver, its benefits and techniques to mitigate the challenges of CAP-based VLC systems.**

***Index Terms*—Multiband Carrierless amplitude and phase modulation ($m$-CAP), visible light communication (VLC), optical wireless communication, light emitting diode (LED), fractionally-spaced equalization (FSE), peak-to-average power (PAPR), synchronization, spatial modulation, subband index modulation.**

## I. Introduction

The current trend to enhance mobile broadband experience with innovative data applications is stretching the limit of existing communication infrastructures. This growing demand in data-intensive applications has further raised the need to explore the optical spectrum to support the overcrowded radio frequency (RF) in providing wireless communication. Visible light communications (VLC), which is attracting growing research interests, is a promising technology in this regard due to its numerous potentials and benefits. These benefits include immunity to electromagnetic interference, low power consumption, high security, unlicensed spectrum and the use of inexpensive devices [1–3].

Visible light communication involves the use of visible light-emitting diodes (LEDs) to provide both illumination and wireless data communication. The main reasons for the use of LEDs for illumination include their high quality, high energy efficiency and longer life span in comparison to other non-solid state lighting devices such as incandescent and fluorescent lamps [4, 5]. Therefore, the widespread adoption of LEDs for illumination together with the rapid advancement in the field of solid state devices have paved the way for the seamless introduction of VLC technology for many applications such as indoor localization, vehicle-to-vehicle communication and many others [6–9]. These rapid advancements have resulted in the development of industry standards for VLC in IEEE 802.15.7 and the ongoing IEEE 802.11bb [10–12].

The main challenge with white-illumination LEDs is the use of phosphor coating in converting the blue wavelengths of LEDs to obtain white phosphor-converted LEDs (PC-LEDs). This approach is cost effective but substantially reduces the modulation bandwidth of PC-LEDs to a few MHz due to the slow phosphorescent relaxation time [13]. Several techniques have been proposed to improve the aggregate data rate for transmission through PC-LEDs. These techniques include the use of blue filter, implementation of equalization techniques and the adoption of spectrally-efficient modulation techniques [14–20].

A modulation technique that has been widely investigated for VLC application is the CAP modulation. This is due to the combination of its high spectral efficiency and implementation simplicity [21]. The CAP scheme has previously been adopted as the standard by asynchronous transfer mode (ATM) standardization body, ATM Forum, and was an early candidate for asymmetric digital subscriber line (ADSL) [22]. It was later discontinued in favour of discrete multitone (DMT) due to its required equalization resources at high throughputs [23]. However, CAP modulation is currently enjoying a resurgence in VLC as a result of its special properties that lead to implementation advantages in optical wireless communication (OWC). Among these properties is that CAP, as a single carrier modulation, has a low peak-to-average power ratio (PAPR) in comparison to discrete multitone (DMT) whose high PAPR is one of its major issues [24]. The low PAPR factor of CAP modulation is well suited to OWC since there is a considerable optical power constraint in the transmitter front-end imposed by both the eye safety regulations and design requirements [24]. In addition, the intensity modulation and direct detection

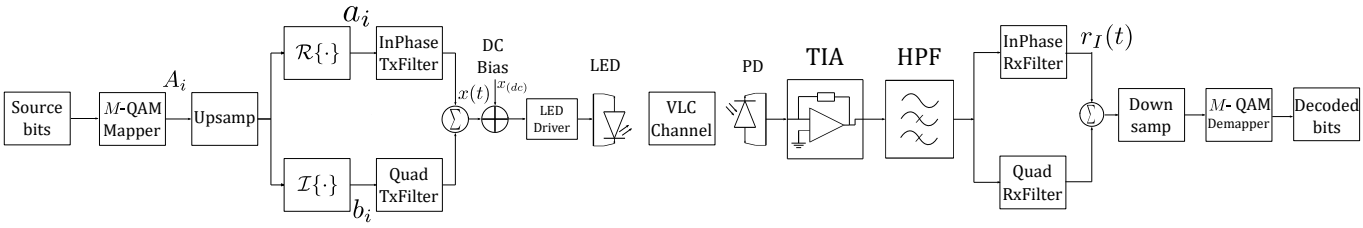


Fig. 1. Schematic block diagram of the CAP modulation scheme.

(IM/DD) technique is used in VLC as a feasible transceiver approach because LEDs are incoherent light sources which makes it difficult to design an efficient coherent receiver [25]. Hence, it is the intensity of the optical emitter that is modulated in VLC which constrains the data-carrying signal to be real-valued, unipolar and non-negative. The CAP signal is real-valued and as such avoids any extra processing techniques such as the Hermitian symmetry in DMT [26]. Furthermore, the CAP transceiver is relatively easy to implement as it uses digital finite impulse response (FIR) filter and avoids the need for carrier modulation and recovery in comparison to its QAM counterpart [21].

However, the CAP-based VLC is not devoid of challenges. The use of orthogonal filters for pulse-shaping and matched filtering operations in the CAP transceiver significantly increase its sensitivity to timing jitter [27]. Furthermore, CAP performance degrades in channels with a non-flat frequency response, which is typical of VLC systems employing PC-LEDs as the transmitter. Similarly, PC-LEDs suffer from small modulation bandwidth which results in severe inter-symbol interference (ISI) for systems operating at high throughputs. In addition, just like the DMT approach, the multiband version of CAP (*m*-CAP) also suffers from high PAPR. These challenges require the development of novel techniques to benefit from the advantages of CAP modulation.

Hence, a detailed analysis of the fundamentals of CAP implementation along with its benefits, challenges and mitigation techniques is presented in this work. Theoretical analysis, simulations and experimental demonstrations are used in providing a comprehensive study of the CAP scheme as a suitable modulation technique for VLC. The specific contributions of this paper include the following: (*i*) a detailed overview of CAP implementation in VLC applications; (*ii*) presentation of the implementation challenges, including the analysis of the complexity and power requirements, along with corresponding mitigation techniques; and (*iii*) proof of concept experimental demonstrations of the techniques used to mitigate the highlighted CAP-based VLC challenges.

The rest of the paper is organized as follows: The fundamentals of CAP system are described in Section II, Section III discusses the implementation challenges for CAP while some mitigation techniques and design considerations are presented in Section IV. Finally, Section V concludes the paper.

## II. Fundamentals of CAP Implementation

CAP is a multi-level, high order and spectrally-efficient modulation technique that is relatively easy to implement. The block diagram of a CAP transceiver is depicted in Fig. 1. The stream of incoming bits are grouped in blocks of $b$ bits and mapped into one of $M = 2^b$ different complex symbols by the $M$-QAM mapper. Each complex symbol from the mapper output can be represented as $A_i = a_i + jb_i$ where $a_i$ and $b_i$ are the real and imaginary part of the $i$th symbol, respectively. The outputs of the mapper are upsampled sufficiently to match the overall system sampling frequency, $f_s$. The in-phase ($a_i$) and quadrature ($b_i$) components are then fed, respectively, into the in-phase ($p(t)$) and quadrature ($\tilde{p}(t)$) digital pulse-shaping filters. The $p(t)$ and $\tilde{p}(t)$ are realized as the product of a root raised cosine filter (RRC) with a cosine and a sine function, respectively. The filters are orthogonal to each other and form a Hilbert pair having the same amplitude response but differing in phase by 90° [28]. The output of the filters are then summed with a suitable DC bias to make it non-negative. The resulting signal is used to modulate the intensity of the LED for onward transmission through the VLC channel. The radiated optical signal, $s(t)$, can be represented as:

$$s(t) = \beta(x(t) + x_{\text{dc}}) \tag{1}$$

where $\beta$ is the electrical-to-optical conversion coefficient, $x_{\text{dc}}$ is the DC bias and $x(t)$ is the transmitted electrical CAP signal which can be written as:

$$x(t) = \sum_{i=-\infty}^{\infty} [a_i p(t - iT) - b_i \tilde{p}(t - iT)]. \tag{2}$$

The pulse-shaping filters are given by:

$$p(t) = g(t)\cos(\omega_c t) \tag{3}$$

and

$$\tilde{p}(t) = g(t)\sin(\omega_c t) \tag{4}$$

where $g(t)$ is the RRC, $\omega_c = 2\pi f_c$ is the center frequency of the CAP signal and $T$ is the symbol duration.

At the receiver, the transmitted signal $x(t)$ is recovered from the incoming optical radiation by a photodetector (PD) and converted to a voltage signal using a transimpedance amplifier (TIA). The DC component of the recovered electrical signal is suppressed with a high pass filter (HPF). This is then passed to the matched filters that consist of the conjugated, time reversed versions of the transmit pulse-shaping filters. The output of the

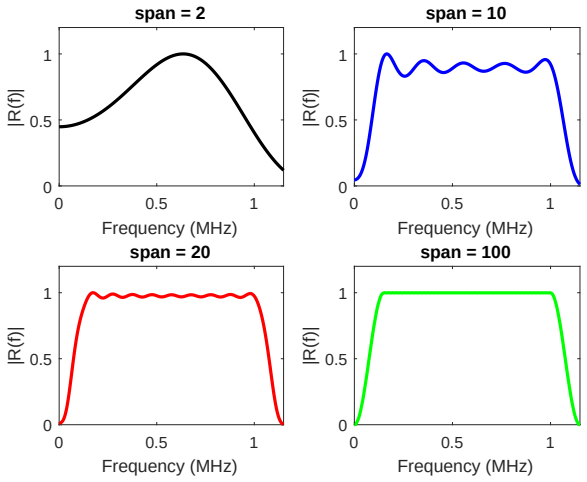


Fig. 2. Magnitude response of the combined in-phase transmit and receive CAP filters for varying values of the filter span, $R_s = 1$ MHz, excess bandwidth, $\alpha = 0.15$ and samples/symbol, $L = 4$.

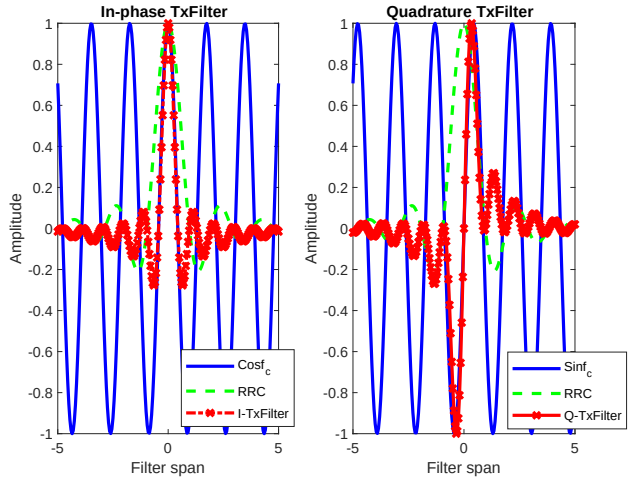


Fig. 3. The impulse response of the $I$ and $Q$ transmit filters for CAP with a span of 10, $\alpha = 0.15$, $L = 20$, $f_s = 20$ MSa/s.

matched filters are then passed through the $M$-QAM demapper for the receiver estimates of the transmitted symbols.

The received electrical signal, with the DC component suppressed, can be represented as:

$$y(t) = \Re P_t h(t) \otimes x(t) + w(t) \tag{5}$$

where $\Re$ is the responsivity of the PD, $P_t$ is the total transmit power, $h(t)$ is the channel attenuation and "$\otimes$" symbol denotes convolution. The $w(t)$ represents the ambient and thermal noise, modelled as additive white Gaussian noise (AWGN) with mean of zero and double-sided spectral density of $N_0/2$ [29].

### A. Design of digital pulse-shaping filters for CAP

The pulse-shaping filter for CAP is often designed in the digital domain. This way, the problem of electronic component drift and tolerance are eliminated, the spectrum characteristics are reproducible without variation and importantly, the digital designs can easily be translated to hardware implementation [30]. Furthermore, the filters are designed as FIR, which are desirable for phase-sensitive applications like data communication.

However, careful selection of the RRC filter parameters is essential to the performance of CAP signal. The main parameters to be designed are the excess bandwidth occupied by the filter pulse (the roll-off factor, $\alpha$), the length of the filter symbol span and the sampling rate, $f_s$ [28, 31]. A high value of $\alpha$ results in more bandwidth usage but leads to better performance [32]. The choice of $\alpha$ in the literature generally varies between $0.1 - 1$ but the value of $\alpha = 0.15$ is widely used for CAP modulation in VLC [28, 31]. An ideal transmit filter requires an infinite symbol span to give zero ISI at the sampling instant when combined with the matched filter at the receiver. However, for practical systems, the span is finite and the filter is truncated. Therefore, the span of the filter is chosen based on the trade-off between computational complexity and performance. The frequency response of the combined transmit and receive in-phase CAP filters is shown in Fig. 2, using samples per symbol $L = 4$ and $\alpha = 0.15$, to highlight the effect of the filter span. It can be observed from the figure that the magnitude response of the combined transmit and receive CAP filters, $|R(f)|$, becomes flat over its spectrum with an increase in the filter span. A span of 10 has been shown to give satisfactory performance for the filter design [31]. The sinusoids frequency, $f_c$, is chosen as the center frequency of the transmitted spectrum and is given as:

$$f_c = \frac{1+\alpha}{2T}. \tag{6}$$

From (6), the upper and lower boundary of the transmitted spectrum can be written as:

$$f_u = f_c + \frac{(1+\alpha)R_s}{2} \tag{7}$$

and

$$f_l = f_c - \frac{(1+\alpha)R_s}{2} \tag{8}$$

respectively where $R_s$ is the symbol rate. In line with the Nyquist sampling requirement, the sampling rate, $f_s$, has to be chosen as:

$$f_s \geq 2f_u. \tag{9}$$

It can be deduced from (9) that the sampling rate is a function of $\alpha$. As $\alpha$ increases from 0 to 1, $f_s$ goes from a minimum of $2R_s$ to $4R_s$. The in-phase and quadrature transmit filters together with their corresponding sinusoids and RRC are presented in Fig. 3 for illustration purposes.

### B. Multi-band CAP

CAP is implemented as a multiband modulation scheme by placing CAP signals on multiple subbands to realize $m$-CAP [31, 38–40]. The main advantage of $m$-CAP is its improved tolerance to channel impairments compared to the single band CAP [31]. By dividing the single wideband CAP into multiple

TABLE I
SUMMARY OF THE EXPERIMENTAL DEMONSTRATIONS RESULTS FOR CAP IN VLC APPLICATIONS.

| Year | Data rate | Transmitter | Equalization | BER | Distance | Ref |
|---|---|---|---|---|---|---|
| 2015 | 8 Gb/s | RGBY LED with WDM | Pre and Post | $< 3.8 \times 10^{-3}$ | 1 m | [33] |
| 2015 | 4.5 Gb/s | RGB LED with WDM | Pre and Post | $< 3.8 \times 10^{-3}$ | 1.5 m | [34] |
| 2015 | 4.5 Gb/s | RGB LED with WDM | Pre and Post | $< 3.8 \times 10^{-3}$ | 1.1 m | [16] |
| 2014 | 1.35 Gb/s | RGB LED with WDM | Pre and Post | $< 3.8 \times 10^{-3}$ | 0.3 m | [35] |
| 2013 | 3.22 Gb/s | RGB LED with WDM | Pre and Post | $< 1 \times 10^{-3}$ | 0.25 m | [36] |
| 2013 | 1.32 Gb/s | Blue LED | Pre and Post | $< 1 \times 10^{-3}$ | 0.25 m | [36] |
| 2012 | 1.1 Gb/s | White LED | Pre and Post | $< 1 \times 10^{-3}$ | 0.23 m | [37] |

narrow subbands, an approximation of a flat frequency response can be realized in each subband for $m$-CAP when transmitted over a frequency selective channel. Furthermore, it circumvents the problem of generating wideband filters and leads to improved bit error rate (BER) performance [31]. The center frequency of the $n$th subband can be expressed as:

$$f_{c,n} = (2n-1)f_c \qquad n = 1, 2, \cdots, m \tag{10}$$

where the $\{f_{c,n}\}$ are chosen to prevent overlap between the subbands and are harmonics of the fundamental subband $f_c$. This observation is very important as it explains the increasing PAPR of $m$-CAP that is discussed in Section III-C. The frequency responses of the subbands for different configurations of $m$-CAP are shown in Fig. 4 [39]. Other benefits of $m$-CAP include the possibility of achieving the Nyquist sampling rate as shown in [31].

### C. Comparison of CAP with other Modulation Schemes

The simplicity of the physical implementation of CAP is derived from its use of digital FIR filters to realize orthogonal channels, which eliminate the need for explicit modulation and demodulation blocks. This is unlike its passband quadrature amplitude modulation (QAM) counterpart that requires a local oscillator (LO) to generate the sine and cosine functions needed for its modulation and demodulation blocks. In addition, the LO signal at the QAM coherent receiver must be aligned with that of the transmitter, both in phase and frequency, using a phase-locked loop (PLL) to ensure a successful carrier recovery. Failure to do this results in lack of synchronization in the QAM transceiver and leads to BER performance degradation. However, as shown in Fig. 1, the modulation/demodulation blocks have been integrated into the pulse-shaping/match filtering blocks in the CAP transceiver. This removes the necessity of having to modulate the CAP baseband signal onto quadrature carriers, hence eliminating the need for carrier recovery, LO and PLL at the receiver. In addition, since the symbol rate and carrier frequency are usually of the same order, the CAP filters can be realised with a reasonably small number of taps [41]. Hence, the main advantage of CAP over QAM is its simpler implementation [21, 42].

The PAPR of CAP has been compared to that of pulse amplitude modulation (PAM) and DMT in the literature [14, 26, 32, 43]. It is shown that the PAPR of CAP is lower when compared with that of DMT but higher in comparison to PAM. This results in advantage when LED non-linearity and the effect of signal clipping are taken into consideration, especially at high modulation orders. Furthermore, the BER performance of CAP has also been compared to that of DMT and PAM [20, 44–46]. Apart from the implementation simplicity and lower PAPR, CAP also has better BER and data

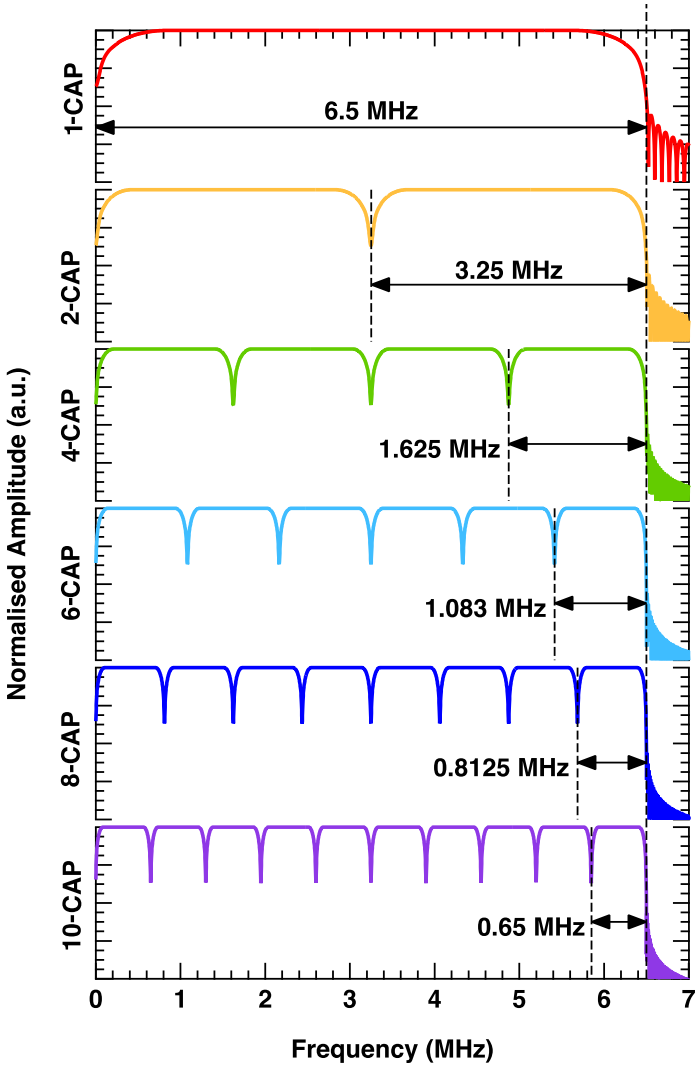


Fig. 4. Frequency responses of the subbands for different configurations of $m$-CAP [39].

rate performance in comparison to DMT in the same physical link [20, 45]. Employing only the blue chip of an RGB-LED at a BER of $10^{-3}$, CAP demonstrates a superior data rate of 1.32 Gb/s in comparison to 1.08Gb/s for DMT [20]. With all the three chips employed, CAP demonstrates a superior data rate of 3.22 Gb/s in comparison to 2.93 Gb/s for DMT [20]. Also, DMT has been found to exhibit a substantially worse performance than CAP in a VLC link employing a white phosphorescent LED [45]. Some of the main reasons for the DMT performance are its low tolerance to the non-linearity of LED and signal clipping [45]. However, at very high data rates, CAP requires complex equalization techniques that increase its complexity in comparison to DMT, which requires a simple single-tap equalizer [47]. The summary of the performance of CAP in VLC experimental demonstrations, as reported in the literature, is given in Table I.

## III. Implementation Challenges for CAP Modulation Technique

The challenges that are encountered in the implementation of CAP-based VLC systems are discussed in this section. The focus is directed at four major aspects of the CAP modulation technique. These are: (*i*) sensitivity to timing jitter, (*ii*) effect of limited modulation bandwidth of the LED, (*iii*) power requirement and (*iv*) computational complexity. Some recently introduced techniques and approaches that address these challenges, with various tradeoffs, are discussed in Section IV.

### A. CAP Sensitivity to Timing Jitter

Timing jitter, one of the challenges of CAP modulation, has been identified as a major impediment to achieving high data rates in optical systems [48]. The reasons for the jitter sensitivity exhibited by the CAP modulation technique can be found in the analysis of its receiver architecture [49]. The matched filter output at the receiver has two components corresponding to the in-phase (in-phase Rx filter) and the quadrature (quadrature Rx filter) arms. In the absence of noise and link attenuation, referring to Fig. 1, the in-phase arm of the matched filter output can be expressed as follows [21]:

$$r_I(t) = x(t) \otimes q(t) \tag{11}$$

where

$$q(t) = p(T - t). \tag{12}$$

Then, it follows that:

$$r_I(t) = \sum_{i=-\infty}^{\infty} a_i r_{II}(t - iT) + \sum_{i=-\infty}^{\infty} b_i r_{IQ}(t - iT) \tag{13}$$

where the desired and the interference parts are respectively given as:

$$r_{II}(t) = p(t) \otimes p(T - t) \text{ and } r_{IQ}(t) = \tilde{p}(t) \otimes p(T - t). \tag{14}$$

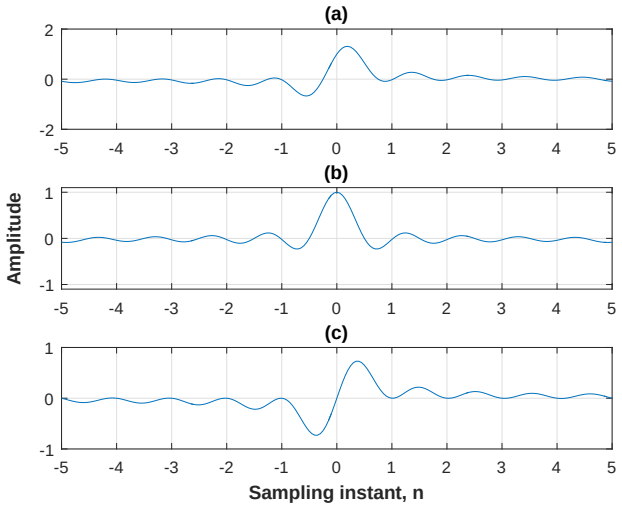


Fig. 5. (a) In-phase arm of the matched filter output of CAP. (b) The desired part; (c) The interference part.

From (14), the desired part can be further expanded as:

$$r_{II}(t) = \int_{-\infty}^{\infty} g(\tau)\cos(\omega_c\tau) \cdot g(\lambda + \tau)\cos(\omega_c(\lambda + \tau))\, d\tau \tag{15}$$

$$= 0.5\cos(\omega_c\lambda) \int_{-\infty}^{\infty} g(\tau)g(\lambda + \tau)\, d\tau + 0.5 \int_{-\infty}^{\infty} g(\tau)g(\lambda + \tau)\cos(\omega_c(\lambda + 2\tau))\, d\tau \tag{16}$$

$$\therefore r_{II}(t) \cong \cos(\omega_c(T - t))r_{ii}(t) \tag{17}$$

where $\lambda = T - t$ and

$$r_{ii}(t) = 0.5[g(t) \otimes g(T - t)]. \tag{18}$$

The second term in (16) can be neglected as it is analogous to filtering a high frequency signal modulated on a sinusoid of frequency ($2\omega_c$) with a low pass filter ($g(t)$). Following the same procedure,

$$r_{IQ}(t) \cong \sin(w_c(T - t))r_{ii}(t). \tag{19}$$

The in-phase arm of the matched filter output ($r_I(t)$), the desired ($r_{II}(t)$) and the interference ($r_{IQ}(t)$) parts are depicted in Fig. 5(a)–(c) respectively for a single transmitted symbol. It can be observed that the desired part, though has its peak at the sampling time $n = 0$, has a very narrow lobe. Also, the interference part contributes no distortion at the sampling instant, but has significant values between sampling instances. This combination increases the sensitivity of CAP signal to timing jitter error and channel impairments as any deviation from the ideal sampling instant leads to taking samples containing significant distortions. Hence, a synchronization technique is a key requirement in the CAP transceiver. A detailed comparison of the CAP and QAM architectures showing that QAM suffers less distortion from the effects of sampling jitter in comparison to CAP has been presented in [21].

### B. CAP Performance under Limited LED Modulation Bandwidth

The frequency response of the PC-LED employed in VLC systems is non-flat over its spectrum. Also, the phosphor coating that is used to convert the emitted light spectrum from blue to white further limits the available modulation bandwidth. The combination of these factors leads to ISI in VLC receivers for high data rate transmission. Additionally, the CAP modulation technique is very sensitive to ISI and requires complex equalizers to achieve good performance in channels with non-flat spectrum [31, 50]. This is the main reason the international telecommunications union (ITU) opted for DMT as the main modulation technique for ATM technology in 1999 [31]. The reason for the high sensitivity of CAP modulation to ISI might be linked to its receiver structure as shown in Fig. 5, which shows that the distortion in a CAP symbol is due to contributions from both its desired and the interference parts. This is in contrast to its QAM counterpart which has a negligible interference part for all $t$ [21]. Therefore, the use of CAP modulation in high throughput LED-based VLC systems requires complex processing techniques to eliminate the effects of the resulting ISI in the received symbols. However, as previously mentioned, $m$-CAP can be conveniently used to mitigate this non-flat response. Techniques such as bit/power loading can be integrated with $m$-CAP to further improve performance.

### C. Power Requirement

The PAPR of an $m$-CAP system merits an important consideration, given its multi-band nature. One of the advantages of single band CAP is its low PAPR. However, for an $m$-CAP modulation scheme, the probability of high peak occurrence increases with increase in the number of subbands. The center frequencies of the $m$-CAP subbands are harmonics of $f_{c,1}$, as such, the subband signals will periodically add up in amplitude during the modulation process. To illustrate this, Fig. 6 shows the transmit filters of an $m$-CAP scheme with three subbands ($m = 3$). It can be observed that the addition of the transmit filters produces a larger amplitude at the sampling instant in comparison to the individual transmit filters. This will increase the likelihood of the occurrence of high PAPR as a result of the coherent addition of the signals in the individual subbands. In order to investigate the $m$-CAP PAPR, we define the PAPR per each transmitted symbol as:

$$PAPR \triangleq \frac{\max\limits_{0\le i\le L-1} |x_i|^2}{E[|x_i|^2]} \tag{20}$$

where $x_i$ is the $i^{\text{th}}$ transmitted $m-$CAP sample while $E[\cdot]$ denotes the statistical expectation. As can be inferred from Fig. 7, the probability that the PAPR will exceed 10 dB is $1.2 \times 10^{-3}$ for $m = 4$ and this increases to $6 \times 10^{-2}$ and $3 \times 10^{-1}$ for $m = 16$ and 64, respectively. This means that out of every 1000 symbols, only 15 are likely to have their PAPR exceeding 10 dB for $m = 4$ as compared to 40 and 700 for $m = 16$ and 64, respectively. Expectedly, the PAPR of the $m$-CAP increases with increasing number of subbands.

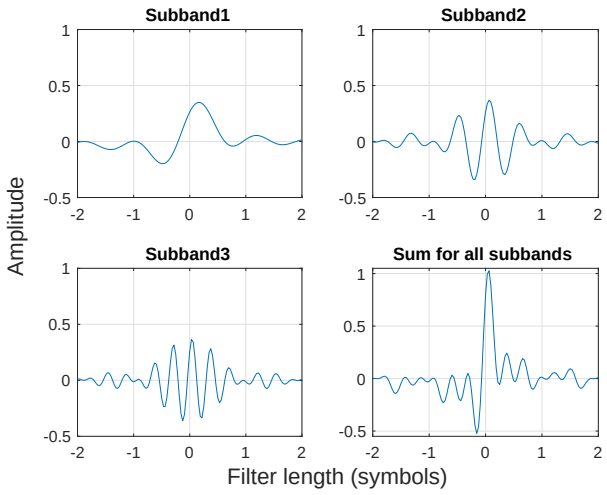


Fig. 6. The quadrature transmit filters of an $m$-CAP scheme and their additions for $m = 3$.

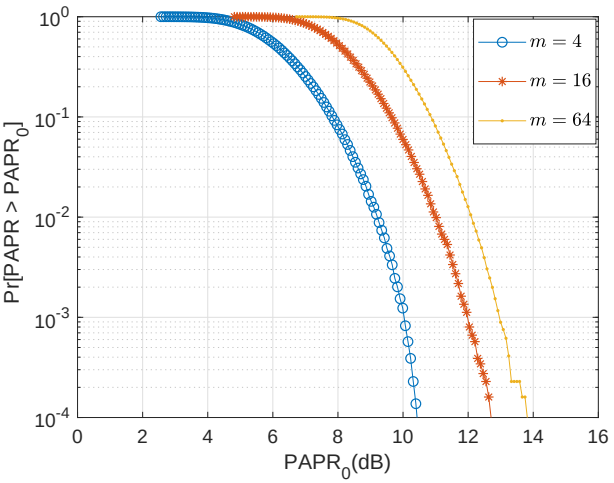


Fig. 7. The CCDF of PAPR of $m-$CAP for different number of subbands using CAP-64.

Thus, the PAPR of $m$-CAP will be an important factor to monitor given the power and dynamic range constraints in VLC systems.

### D. Computational complexity

CAP uses 4 FIR filters in its transceiver (FIR filter 'quads'), a pair each for pulse-shaping at the transmitter and matched filtering at the receiver. So there is a need to consider the number of computations involved in a CAP transceiver, especially considering the growing popularity of $m$-CAP. For a CAP system using a filter of length $G$, the number of real multiplications require for its implementation per each transmitted symbol can be calculated from (2), (3), (4) and Fig. 1 as follows:

- The evaluation of either (3) and (4) requires $G$ real multiplications since it involves element-wise multiplication.

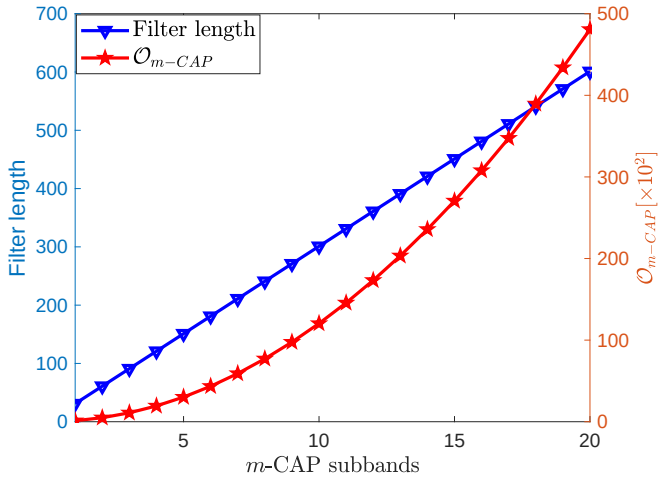


Fig. 8. Complexity dynamics of an $m$-CAP system showing the filter length and the required number of computations as a function of the number of subbands, $m$.

- The pulse-shaping convolution operation of either of the terms on the right hand side of (2) involves another $G$ real multiplications.
- While the matched filtering convolution operation at the receiver in either of the in-phase or quadrature Rx filter of Fig. 1 also involves $G$ real multiplications.

However, the complexity contribution of (3) or (4) is only incurred once and can be done as part of the pre-processing. Hence, the total real multiplications required for the implementation of CAP transceiver is $2(2G)$ per symbol and this can be generalized for an $m-$CAP system as:

$$O_{m\text{-CAP}} = 4Gm. \tag{21}$$

The filter length $G$ is given as:

$$G = G_s L + 1 \tag{22}$$

where $G_s$ is the filter span and $L > 2N(1+\alpha)$ [31]. For the typical values of $G_s = 10$, $\alpha = 0.15$ ($L = 3N$) as proposed in [31], then

$$G = 30m + 1. \tag{23}$$

Substituting (23) for $G$ in (21), the required computational cost per symbol in an $m$-CAP system can be expressed in terms of $m$ as:

$$O_{m\text{-CAP}} = 120m^2 + 4m. \tag{24}$$

Therefore, for a fixed value of $G_s$ and $\alpha$, (23) and (24) respectively provide insight into the complexity dynamics of an $m-$CAP system with regards to the filter length and the required number of computations as more subbands are added. The complexity dynamics is presented in Fig. 8 using (23) and (24). While (23) shows that the filter length of $m$-CAP increases as a linear function of $m$, (24) shows that the $O_{m-\text{CAP}}$ increases as a quadratic function of $m$. This means that $O_{m-\text{CAP}}$ will quickly ramp up as more subbands are added. It follows from (24) that as $m$ increases from 2 to 4 and 16, the $O_{m-\text{CAP}}$ increases in order of magnitude from 3 to 4 and 5, respectively. A compromise is thus needed between increasing the subbands to improve performance and the resulting system complexity.

## IV. Mitigation Techniques for CAP Implementation Challenges

In this section, techniques reported in literature to mitigate the highlighted challenges of CAP are discussed and new ones proposed and demonstrated. The main design consideration in selecting the mitigation techniques is to ensure that the implementation simplicity of the CAP modulation technique is maintained.

### *A. Mitigating Timing Jitter with the 'CAP Filter' Synchronization Technique*

There are two broad categories of solutions to address the timing jitter challenge in CAP. One way is to modify the filter structure of CAP while the other maintains the structure and creates a separate synchronization block. The modified receiver structures from the first set are less-sensitive to timing jitter but results in higher complexity. An example of this is the new sets of two-dimensional (2D) CAP pulses and a set of frequency domain (FD) 3D CAP pulses that are proposed in [51]. The proposed 2D pulses result in improved tolerance to timing jitter but the corresponding BER is worse in the absence of timing jitter. In addition, the proposed FD 3D pulses are more sensitive to timing jitter than the existing CAP pulses. Furthermore, the timing sensitivity solution demonstrated in [52] considered a modified QAM receiver. The proposed receiver, though has low timing sensitivity, results in the loss of the simple linear CAP receiver.

A recent solution, termed the 'CAP filter' synchronization technique, has been proposed that retains the simplicity of CAP by not modifying its generic receiver [49]. The technique uses a synchronization sequence that is derived from the CAP filter with some inherent benefits. The 'CAP filter' synchronization technique maintains the mean value of the transmitted signal and enjoys the benefits of the Nyquist sampling rate of CAP together with the interference elimination of the RRC filter [49]. The maintenance of the average value of the transmitted signal is very important in optical wireless communication due to eye safety regulations. A schematic block diagram of the CAP receiver showing both the location of the synchronizer and its components is presented in Fig. 9. The received signal $\mathbf{y}$ is passed through a correlator along with the sequence $\mathbf{p}$. The correlator output is fed to a threshold detector, which determines the start of the signal, thereby correcting the effect of the timing jitter. The jitter-free or synchronized signal $\mathbf{y_s}$ is then passed to the $m$-CAP demodulator.

The technique has been validated through statistical characterization, simulation and experimental demonstration. In Fig. 10, the effect of varying the sequence length on the performance of the 'CAP filter' synchronization scheme using probability of missed detection (PMD) is illustrated [49]. It can be seen that the PMD improves with

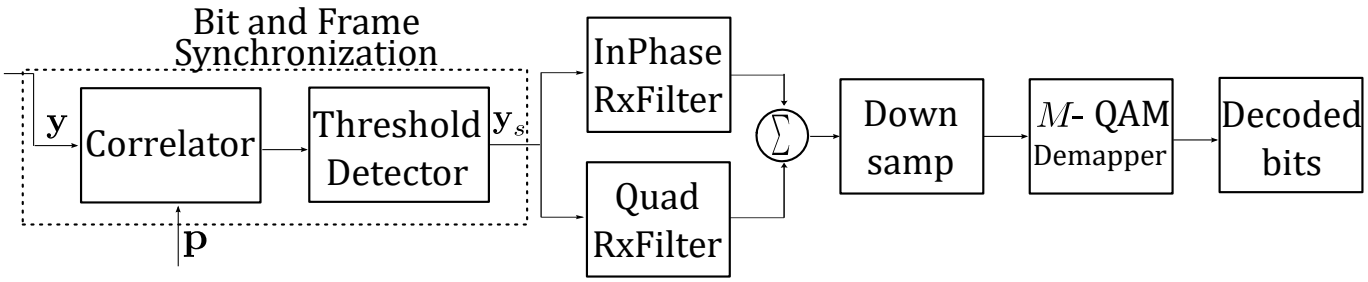


Fig. 9. Schematic block diagram of a simplified CAP receiver showing the location of the synchronizer and its components.

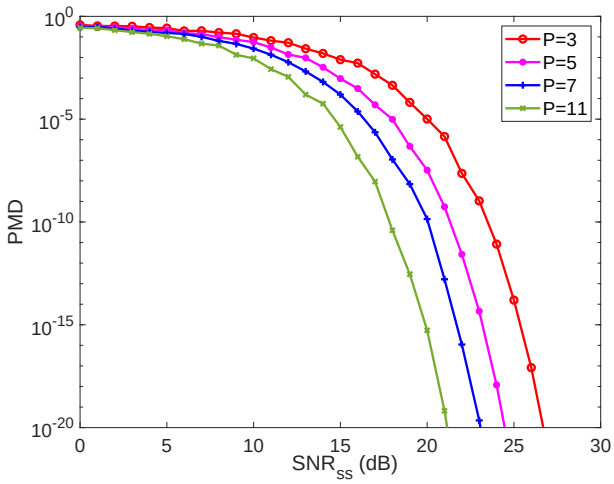


Fig. 10. Probability of missed detection for the 'CAP filter' synchronization technique for different sequence length.

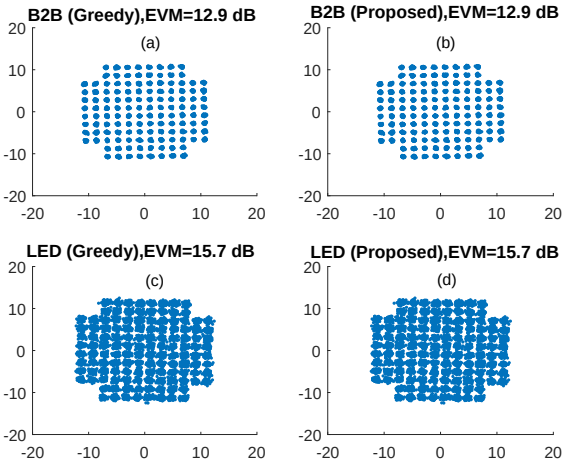


Fig. 12. Constellation diagrams and EVM of the experimental demonstration in VLC for both the 'greedy' and the 'CAP-filter' synchronization algorithm.

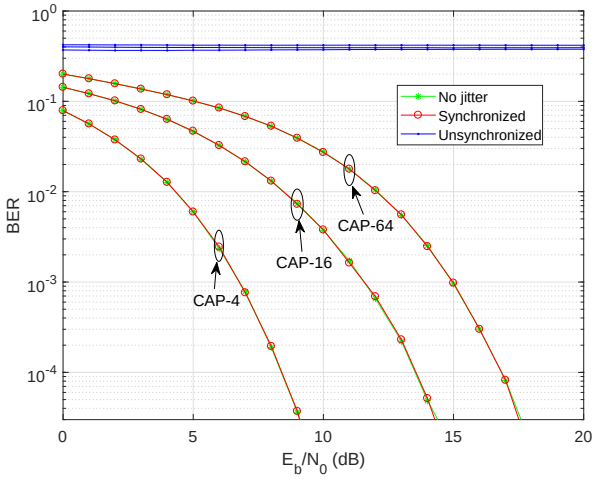


Fig. 11. Comparison of BER performance of CAP with no jitter, with and without synchronization for different constellation sizes in VLC system, $\tau = 0.25T$ and $P = 11$.

increasing sequence length although this results in higher computations. Furthermore, Fig. 11 shows that the 'CAP filter' synchronization is able to correct the effect of timing jitter under VLC bandwidth limitation and achieve a similar BER performance as the ideal case with no timing jitter. Finally, the scheme is validated via experimental demonstration as shown in Fig. 12. Figures 12 (a) and (b) show that the proposed 'CAP filter' synchronization technique achieves identical constellation and error vector magnitude, EVM, of 12.9 dB as the ideal 'greedy' synchronization algorithm in a back-to-back experiment. Similarly, Figs. 12 (c) and (d) show that the proposed 'CAP filter' technique achieves the same constellation and EVM of 15.7 dB as the ideal 'greedy' synchronization in an LED experiment. The results of the simulation and that of the experimental demonstration confirm the effectiveness of the 'CAP filter' synchronization technique for CAP in LED-based VLC systems.

### *B. Mitigating the Effect of Limited Bandwidth and Timing Jitter with a Fractionally-spaced Equalizer*

The majority of the work reported in CAP modulation literature are based on the use of equalization techniques for improving the achievable data rate in LED-based VLC systems [15, 33, 53]. The reported works have concentrated on using symbol-spaced equalizer (SSE) which samples the equalizer inputs at symbol rate and thus have symbol-spaced taps. The

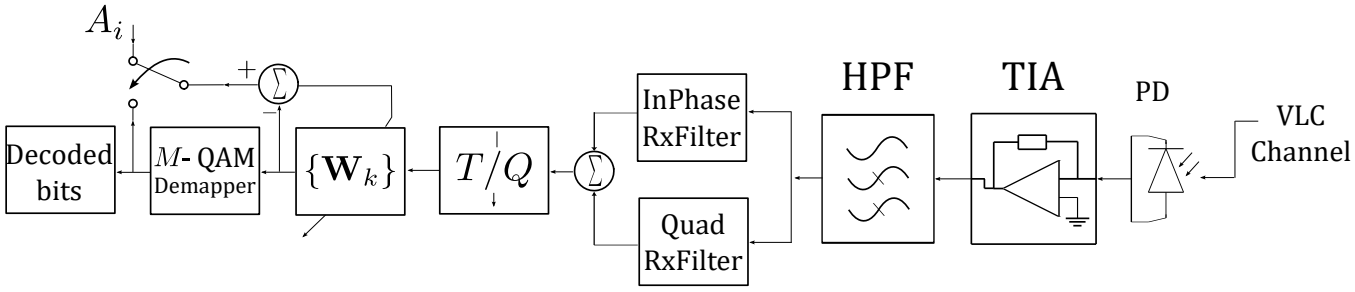


Fig. 13. Schematic block diagram of a simplified CAP transceiver showing the location of the equalizer component.

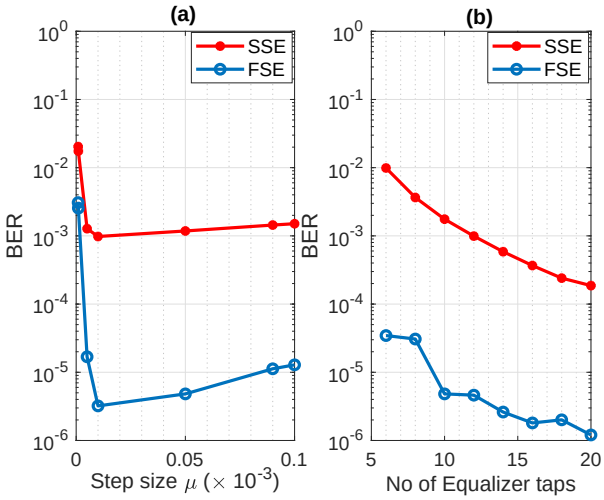


Fig. 14. Sensitivity of the performance of the equalizers to varying step sizes and number of taps, SNR = 15 dB and $R_b$ = 30 Mb/s.

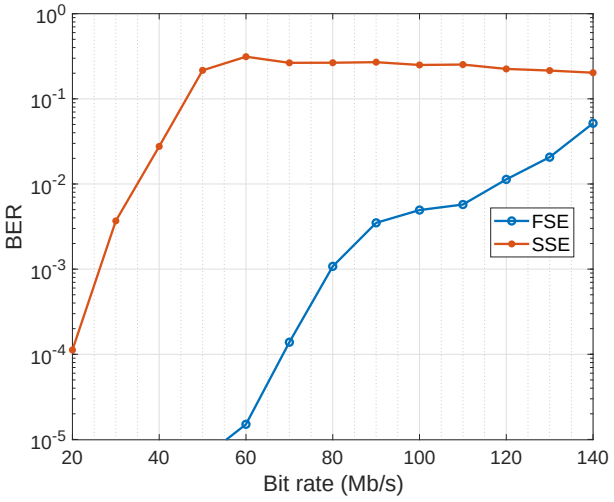


Fig. 16. BER performance of CAP-64 for different data rates at SNR of 20 dB.

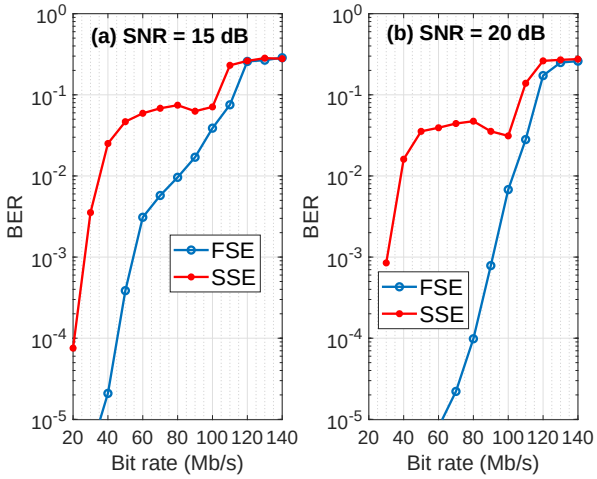


Fig. 15. BER performance of CAP-16 for different data rates at SNR of 15 dB and 20 dB.

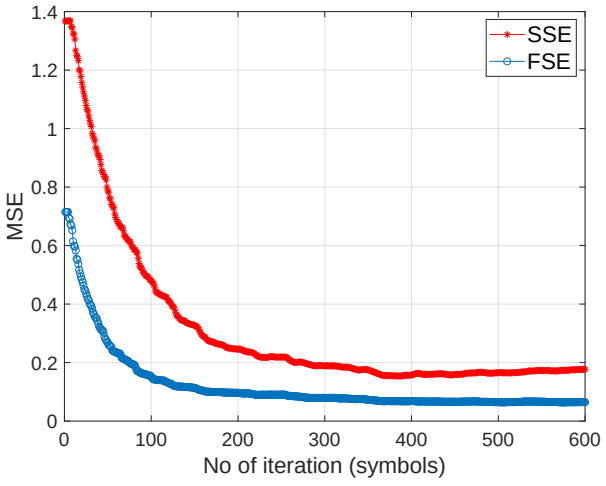


Fig. 17. MSE convergence rate of FSE and SSE for CAP-16 at $R_b$ = 30 Mb/s and SNR=20 dB.

SSE is susceptible to the effect of timing jitter which causes spectrum nulls that result in noise enhancement and potential performance degradation [54]. In contrast, fractionally-spaced equalizers (FSE) circumvent the potential noise enhancement and the resulting performance degradation in SSE by sampling its input at a higher rate of $T' = T/Q$ for $Q > 1$ [55]. Hence, considering the high sensitivity of CAP to timing jitter, SSE is not be the best equalization technique to adopt. Therefore, a comparative performance evaluation of FSE and SSE in joint

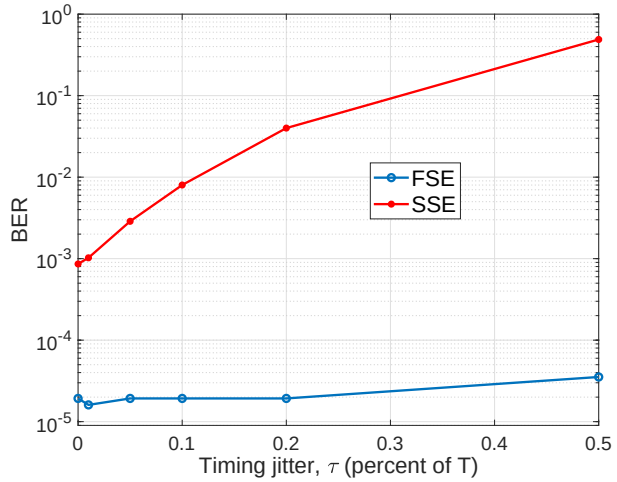


Fig. 18. Comparison of timing jitter mitigation by FSE and SSE using CAP-16 at $R_b$ = 10 Mb/s and SNR = 10 dB.

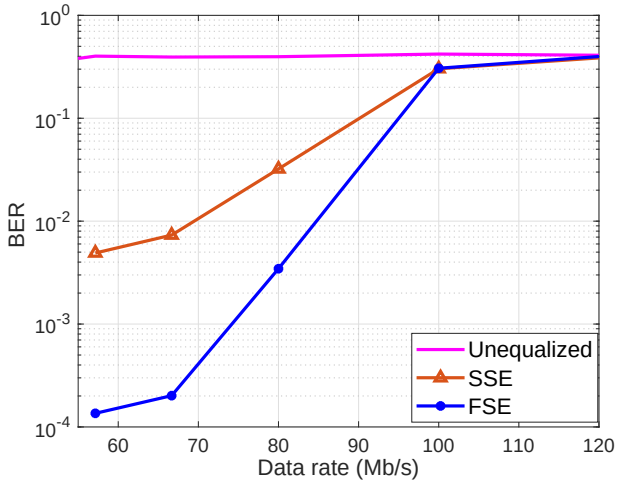


Fig. 19. Experimental demonstration of the BER performance comparison of FSE and SSE using CAP-16 with an OSRAM OSTAR LED that has a -3 dB bandwidth of 6.5 MHz.

mitigation of the effects of timing jitter and limited bandwidth on CAP in LED-based VLC system has been carried out in [55].

It is shown that FSE implementation results in a higher achievable data rate and spectral efficiency, but also reduces the complexity of the overall system by eliminating the need for a separate synchronization block, such as the one considered in Section IV-A. Furthermore, as a proof of concept, an experimental LED-based VLC demonstration is performed to show the advantage of FSE over SSE.

The equalized spectrum for both SSE and FSE can be respectively expressed as [54]:

$$H_T(f) = W_T(f) \sum_i Y\left(f - \frac{i}{T}\right) e^{j2\pi(f-i/T)\tau} \tag{25}$$

and

$$H_{T'}(f) = \sum_i W_{T'}\left(f - \frac{i}{T}\right) Y\left(f - \frac{i}{T}\right) e^{j2\pi(f-i/T)\tau} \tag{26}$$

where $Y(f)$ is the spectrum of the received corrupted signal and $\tau$ is a timing delay. Also, $W_T$ and $W_{T'}$ represent the equalizer weights' spectrum for SSE and FSE, respectively. A comparison of (25) and (26) shows that while (25) is the equalization of the sum of aliased components, (26) is the aliased sum of equalized components. Therefore, FSE is able to compensate for any effect of timing jitter by direct equalization of the received spectrum, which prevents the occurrence of noise enhancement and the possible performance degradation. A simplified CAP transceiver showing the location of the equalizer component, as considered in this work, is presented in Fig. 13.

A least mean square algorithm (LMS) is used to update the equalizer weights due to its low computational complexity. After a preliminary sensitivity study presented in Fig. 14 (a), an optimum step size of $1 \times 10^{-5}$ is chosen. Similarly, Fig. 14 (b) shows that the performance of both equalizers increases with increasing number of taps. Therefore, both equalizers have been implemented using 12 taps to maintain the same computational cost. The oversampling rate of the FSE is chosen to be twice the symbol rate resulting in a $T/2$ FSE.

Figures 15 and 16 show the performance comparison of the $T/2$ FSE and the SSE in a LED-based VLC system. These figures are based on Monte Carlo simulations but the channel response is acquired from a VLC experiment with a white LED. The channel has a non-flat frequency response with a $-3$ dB cut-off frequency of 6.5 MHz. At an SNR of 15 dB and below the forward error correction (FEC) BER limit of $3 \times 10^{-3}$, Fig. 15 (a) shows that FSE is able to achieve a bit rate of 65 Mb/s while SSE only achieves 30 Mb/s resulting in a spectral efficiency ($\eta$) gain of 5.4 bits/s/Hz using CAP-16. For the same constellation size and FEC BER limit, the $\eta$ gain for FSE in comparison to SSE increases to 9.2 bits/s/Hz at an SNR of 20 dB as depicted in Fig. 15 (b).

Furthermore, for a higher constellation size of CAP-64 and at an SNR of 20 dB, Fig. 16 shows that FSE achieves a bit rate of 95 Mb/s compared to 30 Mb/s achieved by SSE. This results in a $\eta$ gain of 10 bits/s/Hz from using FSE. It can therefore be concluded that for the same transmission bandwidth, FSE achieves better data rate and spectra efficiency in comparison to SSE and that the performance advantage increases with increase in SNR and constellation size.

The mean square error (MSE) convergence rate for the two equalizers is shown in Fig. 17 at an SNR of 20 dB and $R_b$ = 30 Mb/s. The FSE offers faster convergence rate and a lower MSE. Faster MSE convergence also implies that a shorter training sequence is required in FSE implementation. It is shown in the figure that the required training sequence for FSE is about 200 symbols while that of SSE is twice that at about 400 symbols.

A further advantage of FSE over SSE for LED-based VLC systems employing CAP modulation is shown in Fig. 18. This figure depicts the performance comparison of FSE and SSE for varying timing jitter using CAP-16. It is shown that FSE performance remains stable while that of SSE suffers severe degradation with increasing timing jitter. These characteristics of FSE to maintain its good performance in the presence of

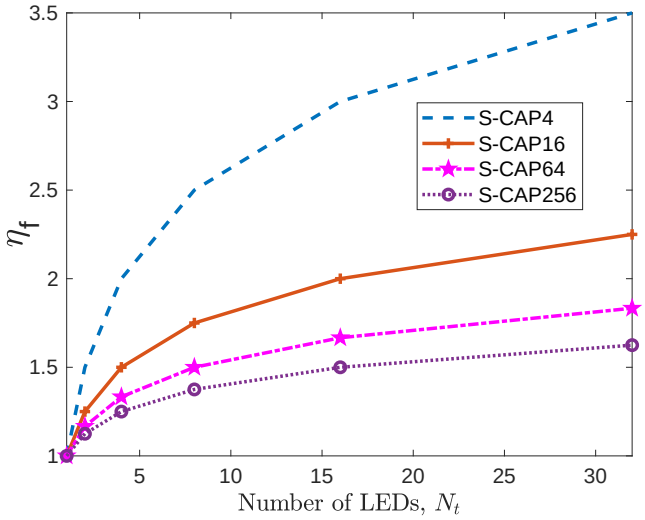


Fig. 20. Spectral efficiency improvement of S-CAP over the conventional CAP scheme for different number of LEDs and constellation sizes.

timing jitter is especially desired for CAP modulation. Hence, it can be argued that FSE implementation is more appropriate to address the timing jitter sensitivity of CAP, as it does not require an extra synchronization block.

An important observation is that both the FSE and SSE have been implemented with the same number of taps (to maintain the same number of computations for both equalizers) and yet, FSE has better performance. Thus, FSE implementation maintains the simplicity of CAP transceiver in LED-based VLC systems, leading to higher achievable spectral efficiency and reduction in both cost and complexity. In addition, since the other techniques such as QAM do not suffer from the effect of timing jitter as much as CAP, the performance gain of FSE will be lower in such techniques.

Finally, as a proof of concept, an experimental LED-based VLC demonstration is carried out to validate the performance advantage of a $T/2$ FSE over SSE for CAP modulation. The transmission distance is 1 m using an OSRAM OSTAR LED with a -3 dB cut-off bandwidth of 6.5 MHz and employing a silicon photodetector (s6967) receiver. The experimental result is presented in Fig. 19 using CAP-16. For the data rates of over 55 Mb/s considered, there is a breakdown of the communication link when no equalization is implemented as depicted in the figure. More importantly, at the FEC BER limit, SSE is only able to achieve a data rate of 55 Mb/s in contrast to 80 Mb/s achieved by FSE. This further validates the conclusion that an FSE is preferred to SSE for CAP-based optical wireless communication systems.

### C. Complexity Reduction for CAP LED-based VLC Systems

The computational complexity of CAP is attributed to both the implementation of its filter and the required equalization scheme at high data rate [47]. The possible use of look-up tables (LUT) at the transmitter have been proposed to reduce the filter implementation complexity, since the filter coefficients are fixed. It has been experimentally demonstrated that over 90% reduction in complexity is achievable at the cost of slight BER degradation when Xia pulses are used to replace the RRC filter that are normally employed for CAP [56]. This is because Xia pulses are full-Nyquist and hence, do not require match filtering. Therefore, by using LUTs at the transmitter and simple sampling at the receiver, significant reduction in complexity is achieved.

Furthermore, the complexity of the equalization scheme can be reduced with the introduction of the spatial modulation (SM) and multiple-input multiple-output (MIMO) techniques [57–59]. These techniques leverage the multiple LEDs that are deployed in VLC to achieve sufficient illumination levels. Using the SM technique, multiple low rate CAP symbols are simultaneously transmitted over an array of available LEDs resulting in a high aggregate data rate at the receiver with low equalization requirement [57]. For a fixed bandwidth, the spatially modulated CAP (S-CAP) transmits more bits/symbol at the transmitter compared to conventional CAP and when the number of bits/symbol is fixed, S-CAP requires lower bandwidth.

The spectral efficiency/bandwidth improvement, $\eta_f$, provided by S-CAP over the conventional CAP is illustrated in Fig. 20 for different constellation sizes $M$ and varying number of LEDS $N_t$. The spectral efficiency improvement increases with increasing $N_t$. Thus, the implementation of S-CAP can lead to lower equalization requirement as it results in less ISI at the receiver.

The S-CAP technique only utilizes some of the available LEDs for spectral efficiency improvement. A scheme that improves on this by utilizing all the available LEDs, either for spectral efficiency or BER improvement, has been proposed in [58] and experimentally demonstrated in [59]. Multiple independent CAP symbols are simultaneously transmitted in a multiple-input multiple-output (MIMO) multiplexing CAP scheme resulting in spectral efficiency improvement by a factor of $N_t$. Alternatively, multiple identical CAP symbols can be simultaneously transmitted in repetitive coded MIMO to improve the BER of the conventional CAP while maintaining the spectral efficiency. For a target BER or data rate at the receiver, the two schemes enable flexible adjustment of the transmitted symbol rate in order to lessen the equalization requirement.

### D. PAPR Reduction for m-CAP Scheme

Unlike single band CAP, the $m$-CAP scheme suffers from increasing PAPR as a result of its multi-band nature. This high PAPR can be reduced by the subband indexing technique proposed in [60]. The subband index CAP (SI-CAP) only modulates some of the $m$-CAP subbands with data information and as such, the unmodulated subbands does not contribute to the resulting PAPR. This results in improved PAPR of SI-CAP. The SI-CAP transmits additional information bits on the indices of the $m$-CAP subbands thereby making up on the lost spectral efficiency which results from nulling some of the subbands. The nature of SI-CAP configuration enables flexibility in design, which could results in spectral efficiency that is greater than the possible $\log_2(M)$ limit in $m$-CAP. It

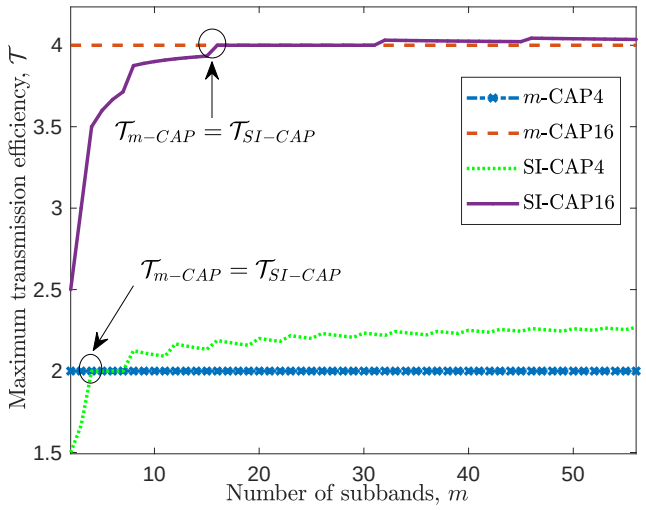


Fig. 21. Comparison of the maximum achievable transmission efficiency of SI-CAP and $m$-CAP as the number of subbands $m$ increases.

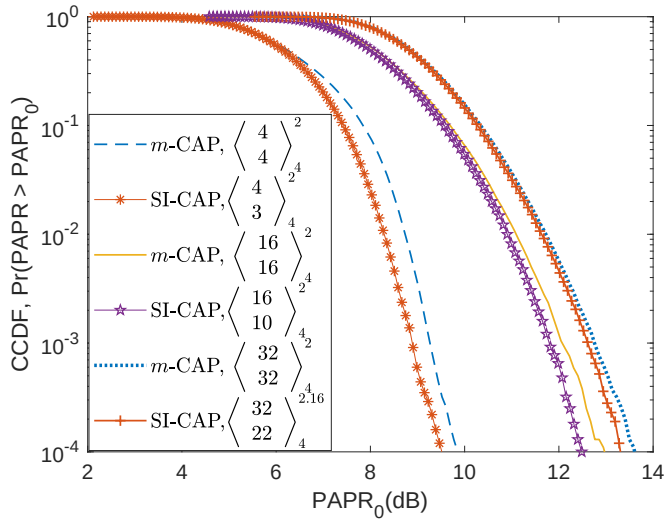


Fig. 22. The comparison of complimentary cumulative density function (CCDF) of the peak to average power ratio (PAPR) of SI-CAP and $m$-CAP for varying number of subbands.

has been shown that the number of bits encoded in SI-CAP symbol in bits per channel use (bpcu) can be expressed as [60]:

$$\mathcal{T}_{\text{SI-CAP}} = \frac{\lfloor \log_2 \left({}^{m}C_{N_a}\right) \rfloor + N_a \log_2(M)}{m} \tag{27}$$

where $N_a$ refers to the number of 'active' modulated subbands by the SI-CAP. Comparison of $\mathcal{T}_{\text{SI-CAP}}$ and $\mathcal{T}_m$-CAP is depicted in Fig. 21 for different constellation sizes. The figure shows that it is possible to achieve a higher $\mathcal{T}$ with SI-CAP for $m \geq M$. The PAPR reduction capability of SI-CAP is demonstrated in Fig. 22, which shows the comparison of the complimentary cumulative density function (CCDF) of the PAPR of SI-CAP and $m$-CAP for varying number of subbands. For example, using $m = 4$, the probability that the PAPR of SI-CAP will exceed 9 dB is $6 \times 10^{-4}$ compared to $3.5 \times 10^{-3}$ obtained for $m$-CAP. This means that the PAPR of 6 out of 10,000 SI-CAP symbols is likely to exceed 9 dB compared to $m$-CAP's 35. The PAPR of SI-CAP can be reduced further by using less number of active subbands which will result in trading off the transmission efficiency to achieve lower PAPR.

### *E. Other Design Considerations and Discussions*

Several technical challenges highlighted must be addressed in order to improve the CAP modulation scheme for VLC applications. In particular, there should be a more rigorous comparison of CAP with other competing technologies to highlight its advantages and disadvantages. Many experimental works have been reported, but not much has been reported in terms of theoretical investigation [20, 45]. In this regard, theoretical analysis quantifying the effect of timing jitter in CAP as well as the effect of multipath remains open research issues. Similarly, the analytical quantification of the effects of signal clipping and LED non-linearity also remain outstanding research problem, especially in view of the high PAPR of the $m$-CAP scheme. The effect of a non-linear system on a multi-carrier input signal can be modelled as an attenuation of the signal plus a non- Gaussian clipping noise component using the central limit and Bussgang theorem [61]. But whether this characterization can be extended to the $m$-CAP scheme requires some investigation, considering its use of RRC filter and the fact that only a few subbands are implemented.

The current analysis for spatial and MIMO CAP as well as SI-CAP all assumed perfect synchronization and line-of-sight (LOS) condition. The analysis can be extended further to obtain expressions that incorporate the effect of non LOS and timing jitter. Furthermore, considering the performance gain of the S-CAP and SI-CAP, a hybrid system can also be developed that combines the two techniques.

Field programmable gate array (FPGA) development is a promising area of research and provides a means of achieving real-time implementation (RTI) of CAP modulation. There has not been much work done on RTI of CAP in the literature compared to other competing schemes [62–64]. The possibility of operating at the Nyquist sampling rate offered by $m$-CAP modulation might be an advantage in hardware implementation, especially for the design of analogue-to-digital converter (ADC) and digital-to-analogue converter (DAC) at high data rates [31]. Other parameters of considerable importance will be the bit resolution and the previously highlighted timing jitter. While a CAP system, being a single carrier, requires low bit resolution [48], $m$-CAP will require higher bit resolution as more subbands are added. Furthermore, the computational cost and power requirements will put significant constraints on the hardware realization and will be crucial in its design. Overall, RTI of CAP on FPGA will enable thorough analysis of the various issues concerning CAP system and the required hardware resources.

## V. Conclusion

Carrierless amplitude and phase modulation is shown to be a competitive, low-complexity and spectrally-efficient

modulation scheme with unique features in VLC applications. It suffers from severe ISI in bandlimited VLC systems and its high sensitivity to timing jitter results in further performance degradation. A separate synchronization circuit could be implemented, at the cost of extra complexity, to address the timing jitter sensitivity or as demonstrated in the literature, fractionally-spaced equalizer (FSE) can be adopted to address both the synchronization and equalization requirement. Multi-band CAP ($m-$CAP) offers the flexibility of tailoring the transmitted CAP signal to the frequency characteristics of VLC channel, which reduces ISI at the cost of extra computational complexity and power. The pertinent challenges of implementing CAP for LED-based VLC systems have been elucidated in this paper and mitigation techniques presented. A summary of the outcome of this paper is as follows: (*i*) CAP has the potential to achieve high data rates with low complexity in VLC systems; (*ii*) while $m$-CAP implementation results in improved BER performance, its increasing complexity and PAPR pose implementation challenges; (*iii*) performance improvement techniques such as low complexity synchronisation and equalisation techniques, spatial and subband index CAP schemes which are presented in the paper are required to maintain the attractive features of CAP. Further investigations are also recommended, especially in the areas of theoretical analysis of CAP and its real time implementation. Finally, this work presents a coherent and comprehensive overview of CAP implementation for LED-based VLC applications.

## REFERENCES


[1] Z. Ghassemlooy, S. Arnon, M. Uysal, Z. Xu, and J. Cheng, "Emerging optical wireless communications-advances and challenges," *IEEE Journal on Selected Areas in Communications*, vol. 33, no. 9, pp. 1738–1749, 2015.

[2] S. Arnon, *Visible Light Communication*. Cambridge University Press, 2015.

[3] H. Haas, "Visible light communication," in *Optical Fiber Communication Conference*. Optical Society of America, 2015, p. Tu2G.5.

[4] D. Karunatilaka, F. Zafar, V. Kalavally, and R. Parthiban, "LED based indoor visible light communications: State of the art," *IEEE Communications Surveys Tutorials*, vol. 17, no. 3, pp. 1649–1678, thirdquarter 2015.

[5] T. Komine and M. Nakagawa, "Fundamental analysis for visible-light communication system using LED lights," *IEEE Transactions on Consumer Electronics*, vol. 50, no. 1, pp. 100–107, Feb 2004.

[6] P. H. Pathak, X. Feng, P. Hu, and P. Mohapatra, "Visible light communication, networking, and sensing: A survey, potential and challenges," *IEEE Communications Surveys Tutorials*, vol. 17, no. 4, pp. 2047–2077, Fourthquarter 2015.

[7] Y. H. Kim, W. A. Cahyadi, and Y. H. Chung, "Experimental demonstration of VLC-based vehicle-to-vehicle communications under fog conditions," *IEEE Photonics Journal*, vol. 7, no. 6, pp. 1–9, 2015.

[8] I. Takai, T. Harada, M. Andoh, K. Yasutomi, K. Kagawa, and S. Kawahito, "Optical vehicle-to-vehicle communication system using LED transmitter and camera receiver," *IEEE Photonics Journal*, vol. 6, no. 5, pp. 1–14, 2014.

[9] A. Sevincer, A. Bhattarai, M. Bilgi, M. Yuksel, and N. Pala, "Lightnets: Smart lighting and mobile optical wireless networks a survey," *IEEE Communications Surveys & Tutorials*, vol. 15, no. 4, pp. 1620–1641.

[10] M. Uysal, F. Miramirkhani, O. Narmanlioglu, T. Baykas, and E. Panayirci, "IEEE 802.15.7r1 reference channel models for visible light communications," *IEEE Communications Magazine*, vol. 55, no. 1, pp. 212–217, January 2017.

[11] "IEEE standard for local and metropolitan area networks–part 15.7: Short-range wireless optical communication using visible light," *IEEE Std 802.15.7-2011*, pp. 1–309, Sept 2011.

[12] "IEEE standard for information technology–telecommunications and information exchange between systems local and metropolitan area networks–specific requirements part 11: Wireless LAN medium access control (MAC) and physical layer (PHY) specifications– amendment: Light communications," *IEEE Std P802.11bb*, pp. 1–1, Jan 2018.

[13] Y. Wang, Y. Wang, N. Chi, J. Yu, and H. Shang, "Demonstration of 575-Mb/s downlink and 225-Mb/s uplink bi-directional SCM-WDM visible light communication using RGB LED and phosphor-based LED," *Opt. Express*, vol. 21, no. 1, pp. 1203–1208, Jan 2013.

[14] G. Stepniak, M. Schppert, and C. A. Bunge, "Advanced modulation formats in phosphorous LED VLC links and the impact of blue filtering," *Journal of Lightwave Technology*, vol. 33, no. 21, pp. 4413–4423, Nov 2015.

[15] Y. Wang and N. Chi, "Investigation of advanced pre- and post-equalization schemes in high-order CAP modulation based high-speed indoor VLC transmission system," pp. 100 190C–100 190C–9, 2016.

[16] Y. Wang, L. Tao, X. Huang, J. Shi, and N. Chi, "Enhanced performance of a high-speed WDM CAP64 VLC system employing Volterra series-based nonlinear equalizer," *IEEE Photonics Journal*, vol. 7, no. 3, pp. 1–7, June 2015.

[17] Y. Wang, X. Huang, L. Tao, and N. Chi, "1.8-Gb/s WDM visible light communication over 50-meter outdoor free space transmission employing CAP modulation and receiver diversity technology," in *2015 Optical Fiber Communications Conference and Exhibition (OFC)*, March 2015, pp. 1–3.

[18] S. W. Wang, F. Chen, L. Liang, S. He, Y. Wang, X. Chen, and W. Lu, "A high-performance blue filter for a white-LED-based visible light communication system," *IEEE Wireless Communications*, vol. 22, no. 2, pp. 61–67, April 2015.

[19] N. Chi, Y. Wang, and X. Huang, "Advancing the capacity of phosphorescent white LED based visible light communication network," in *2015 IEEE Summer Topicals Meeting Series (SUM)*, July 2015, pp. 33–34.

[20] F. M. Wu *et al.*, "Performance comparison of OFDM signal and CAP signal over high capacity RGB-LED-based WDM visible light communication," *IEEE Photonics Journal*, vol. 5, no. 4, pp. 7 901 507–7 901 507, Aug 2013.

[21] A. H. Abdolhamid and D. A. Johns, "A comparison of CAP/QAM architectures," in *Proceedings of the 1998 IEEE International Symposium on Circuits and Systems, 1998. ISCAS'98.*, vol. 4. IEEE, 1998, pp. 316–316.

[22] J. Gao, Y. H. Leung, and V. Sreeram, "Digital filters for carrierless amplitude and phase receivers," in *Proceedings of IEEE Region 10 International Conference on Electrical and Electronic Technology. TENCON 2001 (Cat. No.01CH37239)*, vol. 2, 2001, pp. 575–579 vol.2.

[23] B. R. Saltzberg, "Comparison of single-carrier and multitone digital modulation for ADSL applications," *IEEE Communications magazine*, vol. 36, no. 11, pp. 114–121, 1998.

[24] W. O. Popoola, Z. Ghassemlooy, and B. G. Stewart, "Pilot-assisted PAPR reduction technique for optical OFDM communication systems," *Journal of Lightwave Technology*, vol. 32, no. 7, pp. 1374–1382, 2014.

[25] S. Dimitrov and H. Haas, *Principles of LED Light Communications: Towards Networked Li-Fi*. Cambridge University Press, 2015.

[26] G. Stepniak and J. Siuzdak, "Experimental investigation of PAM, CAP and DMT modulations efficiency over a double-step-index polymer optical fiber," *Optical Fiber Technology*, vol. 20, no. 4, pp. 369 – 373, 2014.

[27] K. O. Akande and W. O. Popoola, "Impact of timing jitter on the performance of carrierless amplitude and phase modulation," in *2016 International Conference for Students on Applied Engineering (ICSAE)*, Oct 2016, pp. 259–263.

[28] G.-H. Im, D. Harman, G. Huang, A. Mandzik, M.-H. Nguyen, and J.-J. Werner, "51.84 Mb/s 16-CAP ATM LAN standard," *IEEE Journal on Selected Areas in Communications*, vol. 13, no. 4, pp. 620–632, 1995.

[29] J. M. Kahn and J. R. Barry, "Wireless infrared communications," *Proceedings of the IEEE*, vol. 85, no. 2, Feb 1997.

[30] K. Gentile, "The care and feeding of digital pulse-shaping filters," *RF DESIGN*, vol. 25, no. 4, pp. 50–58, Oct 2002.

[31] M. I. Olmedo, T. Zuo, J. B. Jensen, Q. Zhong, X. Xu, S. Popov, and I. T. Monroy, "Multiband carrierless amplitude phase modulation for high capacity optical data links," *Journal of Lightwave Technology*, vol. 32, no. 4, pp. 798–804, Feb 2014.

[32] S. Long, M. A. Khalighi, M. Wolf, Z. Ghassemlooy, and S. Bourennane, "Performance of carrier-less amplitude and phase modulation with frequency domain equalization for indoor visible

light communications," in *2015 4th International Workshop on Optical Wireless Communications (IWOW)*, Sept 2015, pp. 16–20.

[33] Y. Wang, L. Tao, X. Huang, J. Shi, and N. Chi, "8-Gb/s RGBY LED-based WDM VLC system employing high-order CAP modulation and hybrid post equalizer," *IEEE Photonics Journal*, vol. 7, no. 6, pp. 1–7, Dec 2015.

[34] Y. Wang, X. Huang, L. Tao, J. Shi, and N. Chi, "4.5-Gb/s RGB-LED based WDM visible light communication system employing CAP modulation and rls based adaptive equalization," *Optics express*, vol. 23, no. 10, pp. 13 626–13 633, 2015.

[35] Y. Wang, L. Tao, Y. Wang, and N. Chi, "High speed WDM VLC system based on multi-band CAP64 with weighted pre-equalization and modified CMMA based post-equalization," *IEEE Communications Letters*, vol. 18, no. 10, pp. 1719–1722, Oct 2014.

[36] F.-M. Wu, C.-T. Lin, C.-C. Wei, C.-W. Chen, Z.-Y. Chen, and H.-T. Huang, "3.22-Gb/s WDM visible light communication of a single RGB LED employing carrier-less amplitude and phase modulation," in *2013 Optical Fiber Communication Conference and Exposition and the National Fiber Optic Engineers Conference (OFC/NFOEC)*, March 2013, pp. 1–3.

[37] F.-M. Wu, C.-T. Lin, C.-C. Wei, C.-W. Chen, H.-T. Huang, and C.-H. Ho, "1.1-Gb/s white-LED-based visible light communication employing carrier-less amplitude and phase modulation," *IEEE photonics technology letters*, vol. 24, no. 19, pp. 1730–1732, 2012.

[38] P. A. Haigh *et al.*, "Multi-band carrier-less amplitude and phase modulation for bandlimited visible light communications systems," *IEEE Wireless Communications*, vol. 22, no. 2, pp. 46–53, April 2015.

[39] P. A. Haigh *et al.*, "A multi-CAP visible-light communications system with 4.85-b/s/Hz spectral efficiency," *IEEE Journal on Selected Areas in Communications*, vol. 33, no. 9, pp. 1771–1779, Sept 2015.

[40] P. A. Haigh *et al.*, "Multi-band carrier-less amplitude and phase modulation for highly bandlimited visible light communications-invited paper," in *2015 International Conference on Wireless Communications Signal Processing (WCSP)*, Oct 2015, pp. 1–5.

[41] F. Sjöberg, "A vdsl tutorial," 2000.

[42] S. Rajbhandari, J. J. D. McKendry, J. Herrnsdorf, H. Chun, G. Faulkner, H. Haas, I. M. Watson, D. OBrien, and M. D. Dawson, "A review of gallium nitride LEDs for multi-gigabit-per-second visible light data communications," *Semiconductor Science and Technology*, vol. 32, no. 2, p. 023001, 2017.

[43] M. A. Khalighi, S. Long, S. Bourennane, and Z. Ghassemlooy, "PAM- and CAP-based transmission schemes for visible-light communications," *IEEE Access*, vol. 5, pp. 27 002–27 013, 2017.

[44] A. Shalash and K. K. Parhi, "Comparison of discrete multitone and carrierless AM/PM techniques for line equalization," in *Circuits and Systems, 1996. ISCAS'96., Connecting the World., 1996 IEEE International Symposium on*, vol. 2. IEEE, 1996, pp. 560–563.

[45] G. Stepniak, L. Maksymiuk, and J. Siuzdak, "Experimental comparison of PAM, CAP, and DMT modulations in phosphorescent white LED transmission link," *IEEE Photonics Journal*, vol. 7, no. 3, pp. 1–8, June 2015.

[46] J. Wei, L. Geng, D. Cunningham, R. Penty, and I. White, "Gigabit NRZ, CAP and optical OFDM systems over POF links using LEDs," *Optics express*, vol. 20, no. 20, pp. 22 284–22 290, 2012.

[47] J. L. Wei, C. Sanchez, and E. Giacoumidis, "Fair comparison of complexity between a multi-band CAP and DMT for data center interconnects," *Opt. Lett.*, vol. 42, no. 19, pp. 3860–3863, Oct 2017.

[48] J. Armstrong, "OFDM for optical communications," *Journal of lightwave technology*, vol. 27, no. 3, pp. 189–204, 2009.

[49] K. O. Akande and W. O. Popoola, "Synchronization of carrierless amplitude and phase modulation in visible light communication," in *2017 IEEE International Conference on Communications Workshops (ICC Workshops)*, May 2017, pp. 156–161.

[50] J. Gao and Y. H. Leung, "A new adaptive equalizer for carrierless amplitude and phase (CAP) receivers," in *Proceedings of the 1999 IEEE International Symposium on Circuits and Systems, 1999. ISCAS '99.*, vol. 3, Jul 1999, pp. 90–93 vol.3.

[51] S. Lin, J. B. Wang, J. Y. Wang, J. Wang, and M. Chen, "Low-timing-sensitivity waveform design for carrierless amplitude and phase modulation in visible light communications," *IET Optoelectronics*, vol. 9, no. 6, pp. 317–324, 2015.

[52] I. L. Thng, A. Cantoni, and Y. H. Leung, "Low timing sensitivity receiver structures for CAP," *IEEE Transactions on Communications*, vol. 48, no. 3, pp. 396–400, 2000.

[53] K. Werfli *et al.*, "Multi-band carrier-less amplitude and phase modulation with decision feedback equalization for bandlimited VLC systems," in *2015 4th International Workshop on Optical Wireless Communications (IWOW)*, Sept 2015, pp. 6–10.

[54] J. G. Proakis, "Adaptive equalization for TDMA digital mobile radio," *IEEE Transactions on Vehicular Technology*, vol. 40, no. 2, pp. 333–341, 1991.

[55] K. O. Akande, P. A. Haigh, and W. O. Popoola, "Joint equalization and synchronization for carrierless amplitude and phase modulation in visible light communication," in *2017 13th International Wireless Communications and Mobile Computing Conference (IWCMC)*, June 2017, pp. 876–881.

[56] P. A. Haigh and I. Darwazeh, "Demonstration of reduced complexity multi-band CAP modulation using Xia-pulses in visible light communications," in *2018 Optical Fiber Communications Conference and Exposition (OFC)*, March 2018, pp. 1–3.

[57] K. O. Akande and W. O. Popoola, "Generalised spatial carrierless amplitude and phase modulation in visible light communication," in *2018 IEEE International Conference on Communications (ICC)*, May 2018, pp. 1–6.

[58] K. O. Akande and W. O. Popoola, "MIMO techniques for carrierless amplitude and phase modulation in visible light communication," *IEEE Communications Letters*, vol. 22, no. 5, pp. 974–977, May 2018.

[59] K. Werfli, P. Chvojka, Z. Ghassemlooy, N. B. Hassan, S. Zvanovec, A. Burton, P. A. Haigh, and M. R. Bhatnagar, "Experimental demonstration of high-speed $4 \times 4$ imaging multi-CAP MIMO visible light communications," *Journal of Lightwave Technology*, vol. 36, no. 10, pp. 1944–1951, May 2018.

[60] K. O. Akande and W. O. Popoola, "Subband index carrierless amplitude and phase modulation for optical communications," *Journal of Lightwave Technology*, vol. 36, no. 18, pp. 4190–4197, Sept 2018.

[61] S. Dimitrov, S. Sinanovic, and H. Haas, "Clipping noise in OFDM-based optical wireless communication systems," *IEEE Transactions on Communications*, vol. 60, no. 4, pp. 1072–1081, April 2012.

[62] Y. Mao, X. Jin, W. Liu, C. Gong, and Z. Xu, "Demonstration of real-time CAP transceivers with hybrid digital equalization for visible light communication," in *Asia Communications and Photonics Conference*. Optical Society of America, 2017, p. M1G.4.

[63] J. Shi, X. Huang, Y. Wang, and N. Chi, "Real-time bi-directional visible light communication system utilizing a phosphor-based LED and RGB LED," in *2014 Sixth International Conference on Wireless Communications and Signal Processing (WCSP)*, Oct 2014, pp. 1–5.

[64] C.-H. Yeh, Y.-L. Liu, and C.-W. Chow, "Real-time white-light phosphor-LED visible light communication VLC with compact size," *Optics express*, vol. 21, no. 22, pp. 26 192–26 197, 2013.